Appl. Math. Mech. -Engl. Ed., **44**(11), 1887–1910 (2023)

APPLIED MATHEMATICS AND MECHANICS (ENGLISH EDITION)

https://doi.org/10.1007/s10483-023-3047-6

A novel adaptive harmonic balance method with an asymptotic harmonic selection*

Rongzhou LIN[1], Lei HOU[1,†], Yi CHEN[1], Yuhong JIN[1], N. A. SAEED[2,3,4], Yushu CHEN[1]

1. School of Astronautics, Harbin Institute of Technology, Harbin 150001, China;
2. Department of Physics and Engineering Mathematics, Faculty of Electronic Engineering, Menoufia University, Menouf 32952, Egypt;
3. Department of Automation, Biomechanics, and Mechatronics, Faculty of Mechanical Engineering, Lodz University of Technology, Lodz 90924, Poland;
4. Mathematics Department, Faculty of Science, Galala University, Galala 43511, Egypt

(Received Jun. 2, 2023 / Revised Sept. 10, 2023)

Abstract The harmonic balance method (HBM) is one of the most widely used methods in solving nonlinear vibration problems, and its accuracy and computational efficiency largely depend on the number of the harmonics selected. The adaptive harmonic balance (AHB) method is an improved HBM method. This paper presents a modified AHB method with the asymptotic harmonic selection (AHS) procedure. This new harmonic selection procedure selects harmonics from the frequency spectra of nonlinear terms instead of estimating the contribution of each harmonic to the whole nonlinear response, by which the additional calculation is avoided. A modified continuation method is proposed to deal with the variable size of nonlinear algebraic equations at different values of path parameters, and then all solution branches of the amplitude-frequency response are obtained. Numerical experiments are carried out to verify the performance of the AHB-AHS method. Five typical nonlinear dynamic equations with different types of nonlinearities and excitations are chosen as the illustrative examples. Compared with the classical HBM and Runge-Kutta methods, the proposed AHB-AHS method is of higher accuracy and better convergence. The AHB-AHS method proposed in this paper has the potential to investigate the nonlinear vibrations of complex high-dimensional nonlinear systems.

Key words harmonic balance method (HBM), adaptive harmonic balance (AHB) method, harmonic selection, nonlinear vibration, multi-frequency excitation

∗ Citation: LIN, R. Z., HOU, L., CHEN, Y., JIN, Y. H., SAEED, N. A. and CHEN, Y. S. A novel adaptive harmonic balance method with an asymptotic harmonic selection. *Applied Mathematics and Mechanics* (*English Edition*), **44**(11), 1887–1910 (2023) https://doi.org/10.1007/s10483-023-3047-6

† Corresponding author, E-mail: houlei@hit.edu.cn

Project supported by the National Natural Science Foundation of China (Nos. 11972129 and 12372008), the National Major Science and Technology Projects of China (No. 2017-IV-0008-0045), the Natural Science Foundation of Heilongjiang Province of China (No. YQ2022A008), the Fundamental Research Funds for the Central Universities of China (No. HIT.OCEF.2023006), the Polish National Science Centre of Poland under the OPUS 18 grant (No. 2019/35/B/ST8/00980), and the Tianjin University Independent Innovation Foundation of China (No. 2023XJS-0038)

Chinese Library Classification O328
2010 Mathematics Subject Classification 00A71, 70K30

1 Introduction

In practical applications, solving nonlinear dynamic equations is a significant part of nonlinear vibration analysis. The mathematical methods can be mainly divided into two parts, i.e., time domain methods and frequency domain methods. Time-domain methods, e.g., the Runge-Kutta method, the Euler method, and the collocation methods[1–3], are widely used to obtain transient responses and steady-state responses, but they are usually time-consuming, especially in high-dimension problems. Frequency domain methods can only provide steady-state responses, but they have great advantages in the calculation efficiency. For most vibration problems, the vibration of engineering systems performs as steady-state responses during operation since transient response decays rapidly due to damping. Therefore, in these cases, frequency domain methods are more suitable than time-domain methods for the vibration characteristics analysis[4–5].

The harmonic balance method (HBM) is a typical frequency-domain method that has been widely used to treat many different types of nonlinearities[6–9]. By representing periodic responses as truncated Fourier series with a set of harmonics, the nonlinear ordinary differential equations in the time domain are transformed into nonlinear algebraic equations in the frequency domain. Then, the approximate analytical solutions can be obtained by solving the above algebraic equations. The bounds of the solution error can be estimated[10]. Therefore, the HBM is more computationally efficient than direct integration methods for getting periodic responses[11]. In order to handle different nonlinear problems, several improvements have been made to modify the HBM. The incremental harmonic balance (IHB) method is developed to analyze parametric instability problems[12–15]. The fast Fourier transform (FFT) is used to improve HBM to avoid repeated calculation of intermediate variables[16–17]. The alternating frequency/time domain (AFT) methods provide an alternative way to calculate periodic responses, and have been widely used in many nonlinear vibration analyses[18–23]. Equipped with continuation such as the arc-length method, the unstable solution can be obtained by the HBM[24–26]. Moreover, the HBM can predict the chaos[7] and be extended to treat large-scale nonlinear systems[27].

Despite the obvious advantages of the HBM, the size of nonlinear algebraic equations is related to the product of the number of the degree of freedom (DOF) as well as the number of harmonics. As a result, the HBM can produce enormous nonlinear algebraic equations when solving high-dimension systems or multi-frequency forced systems, which increases the computing time significantly. Generally, some harmonics contribute less to the exact nonlinear response. If they can be recognized and ignored in advance, the size of nonlinear algebraic equations can be decreased, and then the computing efficiency can be improved. Therefore, a method known as the adaptive harmonic balance (AHB) method is proposed, which can select the necessary harmonics for a given accuracy[11].

The AHB method was first proposed by Gullapalli and Gourary[28] in 2000. The nodal residual norm was used to estimate the contribution of the harmonics, based on which a series of advanced AHB methods were presented[29–34]. Maple et al.[29–30] introduced a new AHB method by examining the fraction of spectral energy to augment frequencies. Zhu and Christoffersen[31] proposed a new AHB method by using the warped multi-time partial differential equation to separate fast and slow criteria in the responses so as to estimate the harmonic contributions. Jaumouillé et al.[32] developed an AHB method to analyze the nonlinear bolted joint models, and introduced the approximate strain energy to identify the necessary harmonics. Grolet and Thouverez[33] proposed an AHB method based on the tangent predictor for adding and removing harmonics. Suess et al.[34] introduced an AHB method to treat the dry friction

damping problem. By means of calculating the spectral energy ratio of each harmonic to the whole response, the harmonics with a ratio greater than a threshold would retain. Gastaldi and Berruti[35] proposed a Jacobian alert algorithm to check the solution at each frequency step and identified whether the higher harmonics should be considered in the solution. Sert and Cigeroglu[36] proposed a two-step pseudo-response based (PRB)-AHB method to estimate the response with no extra computation. The above-mentioned AHB methods actually reduce the number of harmonics so as to decrease the size of the nonlinear algebraic equations. However, they have some limitations. The selection procedure of these methods could estimate the contribution of all harmonics only in a given range. Some methods require solving an approximate solution containing all harmonics as a reference before selecting the harmonics. For example, the method in Ref. [32] employs the approximate strain energy, the method in Ref. [11] uses the nonlinear force vector, and the method in Ref. [33] relies on the predictive vector. When dealing with a wide frequency range, solving a massive nonlinear or linear equation will be necessary. Therefore, it is very inconvenient to solve complex frequency problems that need a wide range of harmonics, e.g., nonlinear systems subjected to multi-frequency excitations. Moreover, in some methods, the number of harmonics is increased until meeting a stopping criterion or reaching the maximum number of harmonics, which only limits the number of harmonics but cannot neglect unnecessary harmonics[11,36].

The motivation of this paper is to develop a new AHB method by introducing the asymptotic harmonic selection (AHS) procedure, which enables us to estimate the contribution of the most necessary harmonics that are generated from nonlinear terms and excitations. The AHS procedure selects harmonics from the frequency spectra of nonlinear terms whose amplitudes are larger than a given threshold. Therefore, the AHS procedure can select several harmonics rather than one harmonic in an iteration, which improves the efficiency of harmonic selection. The division of harmonics and the initial value construction are introduced to avoid recalculation. Moreover, with the variation of the path parameter, the harmonics are changing adaptively, i.e., some harmonics are added, while some harmonics are deleted. Consequently, the nonlinear algebraic equations are different for different path parameters, resulting in the failure of the traditional arc-length continuation method. A modified continuation method is suggested to overcome this limitation. Furthermore, five examples with different types of nonlinearities and external forces are introduced to demonstrate the effectiveness of the proposed AHB-AHS method. It has been proved that the proposed AHB-AHS method is easily programmed, highly efficient, and robust compared with the classical HBM.

2 Modified adaptive harmonic method

2.1 HBM principle

The general second-order differential equation of an n-DOF nonlinear dynamic system can be written as

$$\boldsymbol{M}\ddot{\boldsymbol{x}} + \boldsymbol{C}\dot{\boldsymbol{x}} + \boldsymbol{K}\boldsymbol{x} + \boldsymbol{f}_{\mathrm{N}}(\boldsymbol{x}, \dot{\boldsymbol{x}}, t) = \boldsymbol{f}_{\mathrm{E}}(t), \tag{1}$$

where $\boldsymbol{M}$, $\boldsymbol{C}$, and $\boldsymbol{K}$ are the mass, damping, and stiffness matrices, respectively. $\boldsymbol{x}$ is the displacement vector. $\boldsymbol{f}_{\mathrm{N}}$ is the nonlinear force vector. $\boldsymbol{f}_{\mathrm{E}}$ is the external force vector. If the external force is periodic with the period $T = 2\pi/\omega$, the steady-state solution $\boldsymbol{x}(t)$ to Eq. (1) can be expressed as follows:

$$\boldsymbol{x}(t) = \boldsymbol{a}_0 + \sum_{i=1}^{m} \boldsymbol{a}_i \cos(i\omega t) + \sum_{i=1}^{m} \boldsymbol{b}_i \sin(i\omega t), \tag{2}$$

where $\boldsymbol{a}_0$ is an $n \times 1$ vector containing the bias terms. $\boldsymbol{a}_i$ and $\boldsymbol{b}_i$ are the unknown Fourier coefficients of the ith harmonic of the cosine components and the sine components, respectively.

m is the truncation number of the Fourier series. Meanwhile, the external force $\boldsymbol{f}_{\mathrm{E}}$ can be written as

$$\boldsymbol{f}_{\mathrm{E}}(t)=\boldsymbol{f}_{\mathrm{E0}}+\sum_{i=1}^{m}\boldsymbol{f}_{\mathrm{Ec}i}\cos(i\omega t)+\sum_{i=1}^{m}\boldsymbol{f}_{\mathrm{Es}i}\sin(i\omega t), \tag{3}$$

where $\boldsymbol{f}_{\mathrm{E0}}$ is the bias term vector of the external force. $\boldsymbol{f}_{\mathrm{Ec}i}$ and $\boldsymbol{f}_{\mathrm{Es}i}$ are the coefficient vectors of the sine and cosine components of the ith harmonic, respectively. The nonlinear forces are dependent on not only the time but also the displacement $\boldsymbol{x}$ and its derivatives, which indicates that the Fourier coefficients of $\boldsymbol{f}_{\mathrm{N}}$ are functions dependent on $\boldsymbol{x}$ and $\dot{\boldsymbol{x}}$. Therefore, the coefficients cannot be expressed analytically. The alternate frequency time (AFT) method[37] is introduced to handle this case, and the nonlinear forces and their coefficients can be obtained as follows:

$$\boldsymbol{f}_{\mathrm{N}}(\boldsymbol{x},\dot{\boldsymbol{x}},t)=\boldsymbol{f}_{\mathrm{N0}}+\sum_{i=1}^{m}\boldsymbol{f}_{\mathrm{Nc}i}\cos(i\omega t)+\sum_{i=1}^{m}\boldsymbol{f}_{\mathrm{Ns}i}\sin(i\omega t), \tag{4}$$

$$\boldsymbol{f}_{\mathrm{N0}}=\frac{1}{T}\int_{0}^{T}\boldsymbol{f}_{\mathrm{N}}(\boldsymbol{x},\dot{\boldsymbol{x}},t)\mathrm{d}t, \tag{5}$$

$$\boldsymbol{f}_{\mathrm{Nc}i}=\frac{2}{T}\int_{0}^{T}\boldsymbol{f}_{\mathrm{N}}(\boldsymbol{x},\dot{\boldsymbol{x}},t)\cos(i\omega t)\mathrm{d}t, \tag{6}$$

$$\boldsymbol{f}_{\mathrm{Ns}i}=\frac{2}{T}\int_{0}^{T}\boldsymbol{f}_{\mathrm{N}}(\boldsymbol{x},\dot{\boldsymbol{x}},t)\sin(i\omega t)\mathrm{d}t, \tag{7}$$

where $\boldsymbol{f}_{\mathrm{N0}}$ is the bias term vector of the nonlinear term. $\boldsymbol{f}_{\mathrm{Nc}i}$ and $\boldsymbol{f}_{\mathrm{Ns}i}$ are the coefficients vectors of the sine and cosine components of the ith harmonic, respectively. Substitute Eqs. (2)–(4) into Eq. (1), and balance the coefficients of the bias term and sine and cosine components on both sides. Then, Eq. (1) is converted into $n(2m+1)$ nonlinear algebraic equations with $n(2m+1)$ unknowns. The matrix form of the nonlinear algebraic equations can be represented as follows:

$$\begin{pmatrix}\boldsymbol{K}&\boldsymbol{0}&\boldsymbol{0}&\cdots&\boldsymbol{0}\\ \boldsymbol{0}&\boldsymbol{\Lambda}(\omega)&\boldsymbol{0}&\cdots&\boldsymbol{0}\\ \boldsymbol{0}&\boldsymbol{0}&\boldsymbol{\Lambda}(2\omega)&\cdots&\boldsymbol{0}\\ \vdots&\vdots&\vdots&&\vdots\\ \boldsymbol{0}&\boldsymbol{0}&\boldsymbol{0}&\cdots&\boldsymbol{\Lambda}(m\omega)\end{pmatrix}\begin{pmatrix}\boldsymbol{a}_0\\ \boldsymbol{a}_1\\ \boldsymbol{b}_1\\ \vdots\\ \boldsymbol{a}_m\\ \boldsymbol{b}_m\end{pmatrix}+\begin{pmatrix}\boldsymbol{f}_{\mathrm{N0}}\\ \boldsymbol{f}_{\mathrm{Nc1}}\\ \boldsymbol{f}_{\mathrm{Ns1}}\\ \vdots\\ \boldsymbol{f}_{\mathrm{Nc}m}\\ \boldsymbol{f}_{\mathrm{Ns}m}\end{pmatrix}=\begin{pmatrix}\boldsymbol{f}_{\mathrm{E0}}\\ \boldsymbol{f}_{\mathrm{Ec1}}\\ \boldsymbol{f}_{\mathrm{Es1}}\\ \vdots\\ \boldsymbol{f}_{\mathrm{Ec}m}\\ \boldsymbol{f}_{\mathrm{Es}m}\end{pmatrix}, \tag{8}$$

$$\boldsymbol{\Lambda}(\omega)=\begin{pmatrix}\boldsymbol{K}-\omega^2\boldsymbol{M}&\omega\boldsymbol{C}\\ -\omega\boldsymbol{C}&\boldsymbol{K}-\omega^2\boldsymbol{M}\end{pmatrix}. \tag{9}$$

Equation (8) can be solved by the Newton and quasi-Newton methods[38]. It is obvious that the computation efficiency of the HBM is affected by the scale of the nonlinear algebraic equations, i.e., the $n(2m+1)$ equations. Since n is fixed in a certain system, decreasing m, the number of the harmonics, can decrease the number of the nonlinear algebraic equations and thus improve the computation efficiency. Moreover, for multi-frequency excitation cases, such as ω_1 and ω_2, all combinations of $m\omega_1\pm n\omega_2$ should be determined for precision[39–40], which causes a great deal of computing storage and time. Therefore, it is hoped to use an algorithm that can select the necessary harmonics and neglect the harmonics that do not contribute significantly to the total solution. The adaptive harmonic balance method (AHBM) is proposed based on the requirement.

2.2 AHS procedure

In previous research on the AHBM, a maximum number of harmonics, $N_{\mathrm{h}}^{\mathrm{m}}$, should be taken, and all harmonics from 1 to $N_{\mathrm{h}}^{\mathrm{m}}$ should be evaluated in the contribution to the total solution. The main idea of these methods is to select the necessary harmonics or cut out the unnecessary harmonics from the intervals $(1, 2, 3, \cdots, N_{\mathrm{h}}^{\mathrm{m}})$. However, the repetitive calculation of the responses of the nonlinear systems for various harmonics is computationally expensive, which requires that $N_{\mathrm{h}}^{\mathrm{m}}$ cannot be too large. Therefore, in this study, a new AHS procedure is proposed to overcome the difficulty, which generates the harmonics from the initial harmonics but does not estimate the response of the nonlinear system, so that more than one harmonics can be selected or deleted in one step iteration.

The main idea of the AHS procedure is that the harmonics other than the external excitation frequencies and natural frequencies can only be generated by nonlinear terms. Assume that the harmonics would be generated by nonlinear terms if an approximate solution is efficiently close to the exact solution.

Since the procedure involves Fourier transforms, the sampling frequency f_{s} should be determined at first, and the Nyquist sampling theorem should be satisfied while the aliasing should be avoided[41]. It should be noted that in some cases, it may be necessary to increase the sampling period T to achieve better frequency resolution. For example, when focusing on frequencies around 0.1ω, the sampling period should be increased by 10 times. Therefore, the set of all harmonics can be represented as follows:

$$\Omega_{\mathrm{a}} = \{\omega_i | \omega_i = i \cdot \omega,\ i \in I_{\mathrm{a}}\}, \tag{10}$$

$$I_{\mathrm{a}} = (1, 2, 3, \cdots, f_{\mathrm{s}}), \tag{11}$$

where I_{a} is the index set of the all harmonic set Ω_{a}. Then, an initial harmonic set should be determined by the user as follows:

$$\Omega_0 = \{\omega_i | \omega_i \in \Omega_{\mathrm{a}},\ i \in I_0 \subset I_{\mathrm{a}}\}, \tag{12}$$

where I_0 is the index set. The selection of the initial harmonics is flexible, which is an initial guess. In general, the frequencies of excitations and their multiple can be set as the initial harmonics.

Substitute the initial harmonic Ω_0 into Eq. (8). Then, the approximate solution $\boldsymbol{x}^{(0)}$ can be obtained by solving Eq. (8). In order to generate other harmonics, the terms of the nonlinear force in Eq. (1) are moved to the right side of the equations so that the system is regarded as a linear system driven by the nonlinear terms and external forces, which can be written as

$$\boldsymbol{M}\ddot{\boldsymbol{x}} + \boldsymbol{C}\dot{\boldsymbol{x}} + \boldsymbol{K}\boldsymbol{x} = \boldsymbol{f}_{\mathrm{NE}}(\boldsymbol{x}, \dot{\boldsymbol{x}}, t), \tag{13}$$

$$\boldsymbol{f}_{\mathrm{NE}}(\boldsymbol{x}, \dot{\boldsymbol{x}}, t) = \boldsymbol{f}_{\mathrm{E}}(t) - \boldsymbol{f}_{\mathrm{N}}(\boldsymbol{x}, \dot{\boldsymbol{x}}, t). \tag{14}$$

Since the approximate solution $\boldsymbol{x}^{(0)}$ has been obtained, $\boldsymbol{f}_{\mathrm{NE}}$ can be obtained accordingly. Then, Fourier transforms are applied, and the new harmonic set and its index set can be defined as follows:

$$\Omega_1 = \{\omega_i | \omega_i \in \Omega_{\mathrm{a}},\ p(\omega_i) > \varepsilon\}, \tag{15}$$

$$I_1 = \{i | i \in I_{\mathrm{a}},\ p(\omega_i) > \varepsilon\}, \tag{16}$$

$$p(\omega_i) = f_{\mathrm{locmax}}(F_{\mathrm{FT}}(\boldsymbol{f}_{\mathrm{NE}}(\boldsymbol{x}^{(0)},\ \dot{\boldsymbol{x}}^{(0)},\ t))), \tag{17}$$

where $f_{\mathrm{locmax}}(\cdot)$ is the local maximum function, $F_{\mathrm{FT}}(\cdot)$ is the Fourier transform, and ε is a selected threshold representing the selection precision. It is worth noting that the selection

threshold has a clear physical meaning. The selection threshold ε can be regarded as the user's tolerance error for the force, i.e., the harmonics of the nonlinear forces whose amplitudes are less than the selection threshold will be ignored. In theory, ε should be chosen as small as possible to obtain a more accurate solution. However, in practical applications, it is acceptable to use the maximum amplitude of the nonlinear forces as a reference for selecting ε. For instance, ε can be set to one thousandth of the maximum amplitude of the nonlinear forces. Hence, Ω_1 contains all harmonics where the amplitude of $\boldsymbol{f}_{\mathrm{NE}}$ is the local maximum and is larger than a selected threshold ε in the frequency domain, and I_1 is the index set of Ω_1.

Afterward, the new harmonic set Ω_1 is substituted into Eq. (8), and a new approximate solution $\boldsymbol{x}^{(1)}$ is solved. However, if solving the nonlinear equation from scratch, the recalculation is expensive and unnecessary. Since the solution $\boldsymbol{x}^{(0)}$ is an approximate solution, the solution $\boldsymbol{x}^{(1)}$ can be obtained based on the solution $\boldsymbol{x}^{(0)}$. In other words, the solution $\boldsymbol{x}^{(0)}$ is regarded as the initial value of the new equation with the new harmonic set Ω_1. However, the new harmonic set Ω_1 may differ from the old harmonics set Ω_0. Therefore, the divisions of Ω_1 and Ω_0 are proposed as follows:

$$\Omega_1 = \Omega_{\mathrm{in}} \cup \Omega_{\mathrm{add}}, \quad \Omega_0 = \Omega_{\mathrm{in}} \cup \Omega_{\mathrm{del}}, \tag{18}$$

where Ω_{in} is the intersection of Ω_1 and Ω_0, Ω_{add} is the set of new harmonics, and Ω_{del} is the set of the harmonics which should be deleted, i.e.,

$$\Omega_{\mathrm{in}} = \Omega_1 \cap \Omega_0, \quad \Omega_{\mathrm{add}} = \Omega_1 - \Omega_0, \quad \Omega_{\mathrm{del}} = \Omega_0 - \Omega_1.$$

Analogously, the index set can be divided, and I_{in}, I_{add}, and I_{del} can be defined. As a consequence, an initial value $\boldsymbol{x}_0^{(1)}$ is constructed as follows:

$$\begin{aligned}\boldsymbol{x}_0^{(1)}(t) = {} & \boldsymbol{a}_0^{(0)} + \sum_{i\in I_{\mathrm{in}}} \boldsymbol{a}_i^{(0)} \cos(\omega_i t) + \sum_{i\in I_{\mathrm{in}}} \boldsymbol{b}_i^{(0)} \sin(\omega_i t) \\ & + \sum_{j\in I_{\mathrm{add}}} \boldsymbol{a}_j^{(1)} \cos(\omega_j t) + \sum_{j\in I_{\mathrm{add}}} \boldsymbol{b}_j^{(1)} \sin(\omega_j t).\end{aligned} \tag{19}$$

$\boldsymbol{a}_0^{(0)}$, $\boldsymbol{a}_i^{(0)}$, and $\boldsymbol{b}_i^{(0)}$ are gathered easily from $\boldsymbol{x}^{(0)}$. $\boldsymbol{a}_j^{(1)}$ and $\boldsymbol{b}_j^{(1)}$ are some small values because of the sufficiently approximate solution $\boldsymbol{x}^{(0)}$ so that the new harmonics contribute less than the old harmonics. Of course, the following linear guess is feasible:

$$\boldsymbol{a}_j^{(1)} = \boldsymbol{b}_j^{(1)} = \frac{F(\omega_j)}{\mathrm{diag}(\boldsymbol{K})}, \quad j \in I_{\mathrm{add}}, \tag{20}$$

where $F(\omega_j)$ is the amplitude of the ω_j harmonic. After substituting $\boldsymbol{x}_0^{(1)}(t)$ and Ω_1 into Eq. (8), the solution $\boldsymbol{x}^{(1)}$ is obtained efficiently since most unknowns are approximate to the exact solution, and thus convergence is achieved with a few iterations. Then, a new set Ω_2 will be generated, similar to what Eq. (15) does. A comparison between Ω_1 and Ω_2 can be carried out by means of Eq. (18). If Ω_{add} is an empty set, which suggests no new harmonics, the iteration of the AHS procedure is completed, and the solution $\boldsymbol{x}^{(1)}$ is the solution to Eq. (1) with the harmonic set Ω_1. Otherwise, the iteration continues until Ω_{add} becomes empty. According to the previous derivation, the flowchart of the AHB-AHS method is shown in Fig. 1.

2.3 Continuation for variable harmonics

2.3.1 Traditional arc-length continuation algorithm

The numerical continuation is a technique to compute a consecutive sequence of points that approximate the desired solution branch, e.g., the amplitude-frequency response curve. Consider a smooth function

$$G : \mathbb{R}^{N+1} \to \mathbb{R}^N.$$

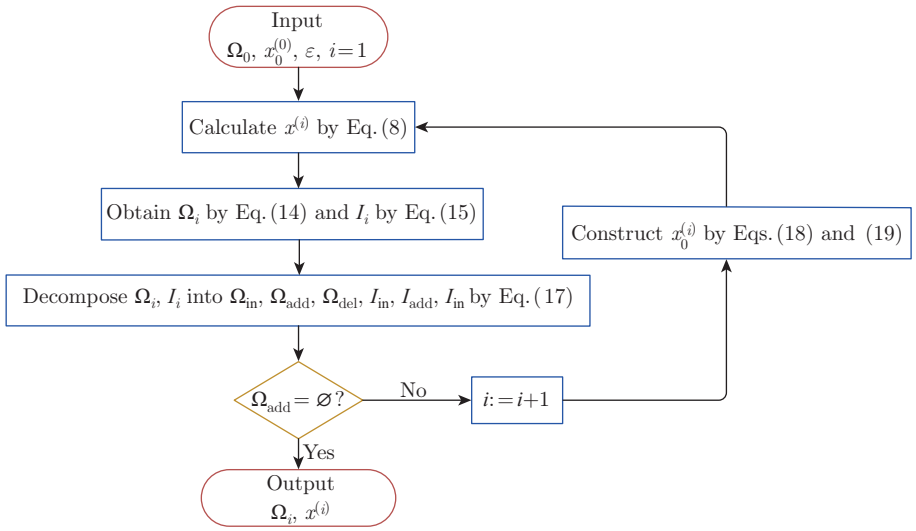

Fig. 1 Flowchart of the AHB-AHS method (color online)

The solution curve is obtained by solving the equation $G(\boldsymbol{y}) = 0$, where $\boldsymbol{y}$ contains the unknowns of Eq. (8) and the path parameter α. Most continuation algorithms implement a predictor-corrector method, which requires the same number of equations as unknowns. Therefore, an extra scalar condition should be applied as

$$G(\boldsymbol{y}) = \boldsymbol{0}, \quad h(\boldsymbol{y}) = 0. \tag{21}$$

A common predictor is the tangent prediction

$$\boldsymbol{Y}^0 = \boldsymbol{y}_i + s\boldsymbol{v}_i, \tag{22}$$

where s is a step-size, and $\boldsymbol{v}_i$ is the normalized tangent vector at $\boldsymbol{y}_i$. One common choice $h(\boldsymbol{y})$ is to find a hyperplane passing through $\boldsymbol{Y}^0$ which is orthogonal to the tangent vector $\boldsymbol{v}_i$,

$$h(\boldsymbol{y}) = \left\langle \boldsymbol{y} - \boldsymbol{Y}^0, \boldsymbol{v}_i \right\rangle = 0. \tag{23}$$

Therefore, the Newton iteration can be expressed as

$$\begin{cases} \boldsymbol{Y}^{k+1} = \boldsymbol{Y}^k - \Phi_y^{-1}(\boldsymbol{Y}^k)\boldsymbol{\Phi}(\boldsymbol{Y}^k), \\ \boldsymbol{\Phi}(\boldsymbol{Y}) = \begin{pmatrix} \boldsymbol{G}(\boldsymbol{y}) \\ \boldsymbol{0} \end{pmatrix}, \\ \boldsymbol{\Phi}_y(\boldsymbol{Y}) = \begin{pmatrix} \boldsymbol{G}_y(\boldsymbol{y}) \\ \boldsymbol{v}_i^{\mathrm{T}} \end{pmatrix}. \end{cases} \tag{24}$$

After Eq. (23) converges, a new point $\boldsymbol{y}_{i+1}$ on the curve is found, and the new tangent vector $\boldsymbol{v}_{i+1}$ should be computed by

$$\begin{pmatrix} \boldsymbol{G}_y(\boldsymbol{y}_{i+1}) \\ \boldsymbol{v}_i^{\mathrm{T}} \end{pmatrix} \boldsymbol{v}_{i+1} = \begin{pmatrix} \boldsymbol{0} \\ a \end{pmatrix}, \tag{25}$$

where $\boldsymbol{G}_y$ is the Jacobian matrix of the function G, and $a > 0$. It is noted that $\boldsymbol{v}_{i+1}$ should be normalized after Eq. (25). In this paper, we choose $a = 1$.

2.3.2 Modified continuation method for harmonics adaptively changing

The traditional continuation is convenient, but it cannot be used in the new AHB method with the AHS procedure, since the size of $\boldsymbol{y}_{i+1}$ is different from the size of $\boldsymbol{y}_i$ when the number of harmonics changes adaptively. Consequently, Eq. (25) is invalid.

In order to handle the predicament, a modification should be used to construct the hyperplane and tangent vector. First of all, it is crucial to classify and discuss the change in the harmonics. It is easy to divide the case into 3 parts, i.e., no changed harmonics, some deleted harmonics, and new generated harmonics. The first situation is trivial because Eq. (25) is available. For the second situation, recall the division of harmonic set by Eq. (18). Then, the unknowns $\boldsymbol{y}_{i+1}$ and tangent vector $\boldsymbol{v}_{i+1}$ are expressed as

$$\begin{cases} \boldsymbol{y}_{i+1} = (\boldsymbol{a}_0, \cdots, \boldsymbol{a}_j, \boldsymbol{b}_j, \cdots, \alpha), & j \in I_0, \\ \boldsymbol{v}_{i+1} = (\boldsymbol{v}_0, \cdots, \boldsymbol{v}_j, \boldsymbol{v}'_j, \cdots, \alpha), & j \in I_0. \end{cases} \tag{26}$$

According to Eq. (18), the new unknowns $\widetilde{\boldsymbol{y}}_{i+1}$ and tangent vector $\widetilde{\boldsymbol{v}}_{i+1}$ after the AHS procedure can be represented as

$$\begin{cases} \widetilde{\boldsymbol{y}}_{i+1} = (\boldsymbol{a}_0, \cdots, \boldsymbol{a}_j, \boldsymbol{b}_j, \cdots, \alpha), & j \in I_{\text{end}}, \\ \widetilde{\boldsymbol{v}}_{i+1} = (\boldsymbol{v}_0, \cdots, \boldsymbol{v}_j, \boldsymbol{v}'_j \cdots, \alpha), & j \in I_{\text{end}}, \end{cases} \tag{27}$$

where I_{end} is the index set of the harmonic set which is converged in the AHS procedure. It is notable that no recalculation occurs to obtain $\widetilde{\boldsymbol{v}}_{i+1}$, but some components of $\boldsymbol{v}_{i+1}$ that belongs to the set $I_0 - I_{\text{end}}$ are deleted.

In the final case, new harmonics are generated after the AHS procedure, and the unknowns can be represented as

$$\widetilde{\boldsymbol{y}}_{i+1} = (\boldsymbol{a}_0, \cdots, \boldsymbol{a}_j, \boldsymbol{b}_j, \cdots, \boldsymbol{a}_k, \boldsymbol{b}_k, \cdots, \alpha), \quad j \in I_{in}, \quad k \in I_{\text{add}}. \tag{28}$$

Because the size of $\widetilde{\boldsymbol{y}}_{i+1}$ is changed and some new harmonics are generated, Eq. (26) is unavailable for computing $\widetilde{\boldsymbol{v}}_{i+1}$. Fortunately, the orthogonality between the hyperplane passing $\widetilde{\boldsymbol{y}}_{i+1}$ and the tangent vector $\widetilde{\boldsymbol{v}}_{i+1}$ still holds. In consequence, the new $\widetilde{\boldsymbol{v}}_{i+1}$ can be obtained by solving

$$G_y(\widetilde{\boldsymbol{y}}_{i+1})\widetilde{\boldsymbol{v}}_{i+1} = \boldsymbol{0}, \tag{29}$$

which means that $\widetilde{\boldsymbol{v}}_{i+1}$ is the null space of the Jacobi matrix G_y. Furthermore, the direction along the curve must be preserved,

$$\widetilde{\boldsymbol{v}}'_{i+1} = \widetilde{\boldsymbol{v}}_{i+1} \cdot \text{sign}(\langle \widetilde{\boldsymbol{v}}_{i+1}, \overline{\boldsymbol{v}}_{i+1} \rangle),$$

where $\overline{\boldsymbol{v}}_{i+1}$ is padded with $\boldsymbol{v}_{i+1}$ and is zero at the corresponding location of generating harmonics so that its length is equal to the length of $\widetilde{\boldsymbol{v}}_{i+1}$. Substitute $\widetilde{\boldsymbol{v}}'_{i+1}$ into Eq. (22), and continue the new predictor-corrector procedure. In addition, if both adding harmonics and deleting harmonics occur together, the harmonics of $\boldsymbol{v}_{i+1}$ should be deleted by Eq. (27) at first, and new harmonics can be added later by Eq. (29).

In summary, the modified arc-length continuation method can be mainly divided into three steps.

Step 1 Obtain the approximate solution $\boldsymbol{y}_{i+1}$ by using Eq. (24) and the approximate tangent vector $\boldsymbol{v}_{i+1}$ by using Eq. (25).

Step 2 Obtain the exact solution $\widetilde{\boldsymbol{y}}_{i+1}$ through the AHS process.

Step 3 Determine the new tangent vector $\widetilde{\boldsymbol{v}}_{i+1}$ by Eq. (29).

Substitute the approximate $\boldsymbol{y}_{i+1}$ into Eq. (25). Then, we obtain an approximate tangent vector $\boldsymbol{v}_{i+1}$ whose direction is the correct continuation direction. However, the tangent vector

$\widetilde{\boldsymbol{v}}_{i+1}$ calculated through Eq. (29) is a correct tangent vector but with an uncertain direction. To address this issue, we use zero-padding to approximate the tangent vector v_{i+1} (denoted with $\overline{\boldsymbol{v}}_{i+1}$ after zero-padding) to ensure

$$\widetilde{\boldsymbol{v}}_{i+1}^{\mathrm{T}}\overline{\boldsymbol{v}}_{i+1} > 0.$$

This is ensured by the fact that the dimension of the null space of the tangent vector belonging to the matrix $\boldsymbol{G}_y$ is 1-dimensional.

3 Numerical examples

In order to examine the proposed AHB-AHS method, five examples featuring different types of nonlinearities and excitations are adopted. The first example is a mathematical pendulum system involving nonlinear sine stiffness subjected to single-frequency external force, and the second one is the same system subjected to double frequency excitations. The third one is the van der Pol system, the fourth one is the nonlinear Mathieu system, and the last one is a dual rotor-bearing system. The efficiency and accuracy of different methods, including the classical HBM, the AHB-AHS method, and the fourth-order Runge-Kutta method (RK4), are compared in each example. All programs are run on the Windows 10 professional operating system with Intel Core i7-8700 CPU and 32 GB RAM. It should be noted that, even though simple models are selected to demonstrate the developed AHB-AHS method, it is applicable to the multiple-DOF system.

3.1 Example 1: generalized pendulum subjected to single frequency excitation

Consider a generalized mathematical pendulum subjected to single frequency excitation described by

$$\ddot{x} + 0.01\dot{x} + 7x + 5\sin x = 0.2\cos(\omega t). \tag{30}$$

This system can be reduced to the Duffing equation by applying Taylor expansion to the nonlinear term. Set the initial harmonics set as $\Omega_0 = \{\omega\}$, the selected threshold ε is 0.001, and the sampling frequency is 128 Hz. For the classical HBM, the 20-harmonic truncation is applied. The amplitude-frequency response curve generated by the classical HBM, AHB-AHS method, and RK4 are shown in Fig. 2.

Since it is difficult for the RK4 to obtain the unstable solution, the curve attained by the RK4 is different from the curves attained by the classical HBM and AHB-AHS method, while

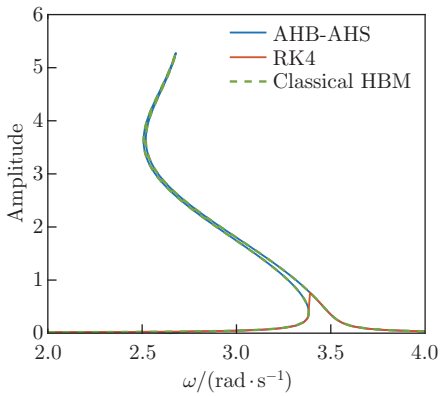

Fig. 2 Amplitude-frequency response curves of the generalized mathematical pendulum system subjected to single frequency excitation (color online)

the curve of the AHB-AHS method almost coincides with that of the classical HBM. The time history at different frequencies of excitations is shown in Fig. 3, the solution of the AHB-AHS method agrees well with the solutions of the classical HBM and RK4. In order to compare the accuracy of the classical HBM and AHB-AHS method, the mean-square difference error (E_{MD}) is used as follows:

$$E_{\mathrm{MD}} = \|x - \widetilde{x}\|_2, \tag{31}$$

where $\|\cdot\|_2$ is the Euclidean norm of the vector, and x and $\widetilde{x}$ are the solutions from the AHB-AHS method and the classical HBM, respectively. The mean-square difference error between the results from the AHB-AHS method and the classical HBM is shown in Fig. 4. The abscissa is the number of continuation iterations rather than the frequency ω because of the bend amplitude-frequency curve so that the frequency is not monotonous. It can be seen that the mean-square difference errors are less than 1×10^{-8} at most frequencies. However, when the frequency is near the frequencies of the peaks, the mean-square difference error grows up to about 1.4×10^{-8}.

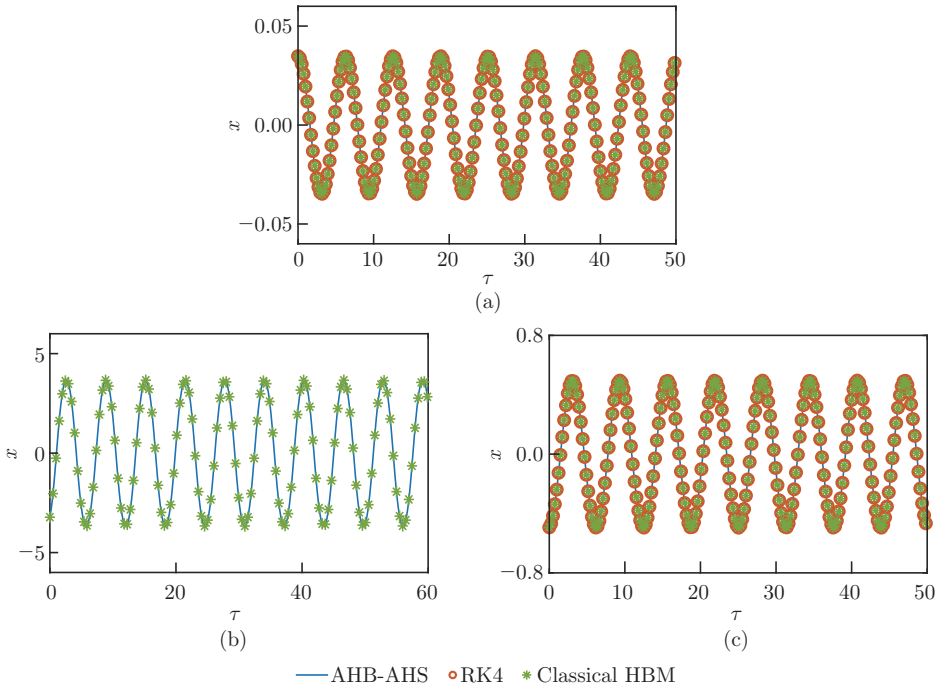

Fig. 3 Time history diagrams of different frequencies subjected to single frequency excitation: (a) $\omega = 2.5\,\mathrm{rad/s}$, (b) $\omega = 2.678\,\mathrm{rad/s}$ at the top of the 1st resonant peak, and (c) $\omega = 3.5\,\mathrm{rad/s}$ (color online)

It is significant to find out the reason for the growth of the mean-square difference error between the AHB-AHS method and the classical HBM. Because the set of harmonics changes with the frequency of external force, the harmonics that have been selected in every continuation iteration are shown in Fig. 5. It is shown that the harmonic set becomes $\{1\omega, 3\omega\}$ from $\{\omega\}$ when $\omega = 3.31\,\mathrm{rad/s}$. Then, the size of the harmonic set increases as ω changes (see Fig. 2). The harmonics of the set increase to $\{\omega, 3\omega, 5\omega, \cdots, 17\omega\}$ at $\omega = 2.68\,\mathrm{rad/s}$, which is the top of the resonant peak shown in Fig. 2. Finally, the harmonics decrease to $\{\omega\}$. From Figs. 4 and 5, we can see that the maximum of E_{MD} is at the top of the peak, which is reasonable since the mean-square difference error represents an absolute error.

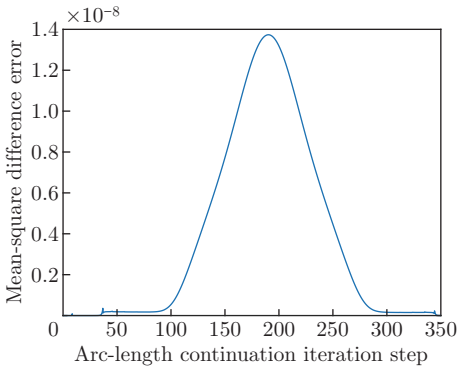

Fig. 4 Mean-square difference error of the amplitude-frequency responses obtained by the AHB-AHS method and the classical HBM subjected to single frequency excitation (color online)

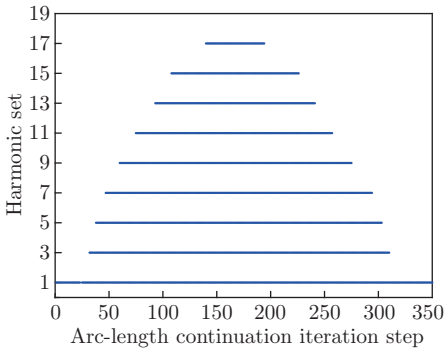

Fig. 5 Variation of the harmonic set subjected to single frequency excitation (color online)

As for the calculation time, it takes 1.081 s for the AHB-AHS method to solve the whole amplitude-frequency response curve, while the classical HBM spends 1.448 s and the RK4 spends 77.732 s. Therefore, the reduction in computational time is 25.4% approximately. The calculation time of different methods is listed in Table 1.

Table 1 Calculation time for obtaining the amplitude-frequency curve of the generalized mathematical pendulum system subjected to single frequency excitation

Method	Calculation time/s	Harmonic set
AHB-AHS	1.081	Adaptive
Classical HBM	1.448	$\{\omega, 2\omega, \cdots, 18\omega\}$
RK4	77.732	–

3.2 Example 2: generalized pendulum subjected to double frequency excitations

Consider a generalized mathematical pendulum subjected to double frequency excitation described by

$$\ddot{x} + 0.01\dot{x} + 7x + 5\sin x = 0.2\cos(\omega t) + 0.1\sin(1.3\omega t). \tag{32}$$

The difference between Eq. (32) and Eq. (30) is the new external force with 1.3ω as frequency. It is difficult to set proper harmonics for the classical HBM because all harmonics of $m\omega \pm n1.3\omega$ should be set. As for the AHB-AHS method, the initial harmonic set is $\{\omega, 1.3\omega\}$. Meanwhile, the integration period T should be expanded to 10 times. The amplitude-frequency response curve and time history diagrams are shown in Fig. 6 and Fig. 7. It can be seen that the curve generated by the AHB-AHS method is close to the classical HBM and coincides with that of the RK4 outside the resonant region. In the resonant region, the solution of the AHB-AHS method agrees with the solution of the classical HBM. The mean-square difference error between the results from the AHB-AHS method and the classical HBM is shown in Fig. 8. The maximum of E_{MD} is less than 2.5×10^{-7}.

Similarly, the selected harmonics at different frequencies are shown in Fig. 9. It can be seen that the number of selected harmonics increases at the resonant region. During the first

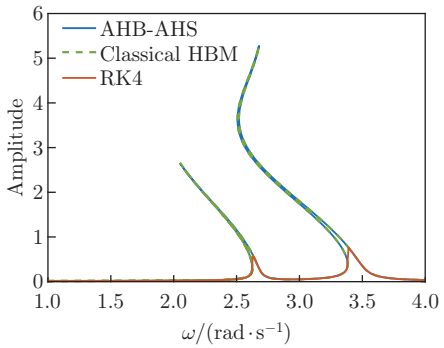

Fig. 6 Amplitude-frequency response curves of the generalized mathematical pendulum system subjected to double frequency excitations (color online)

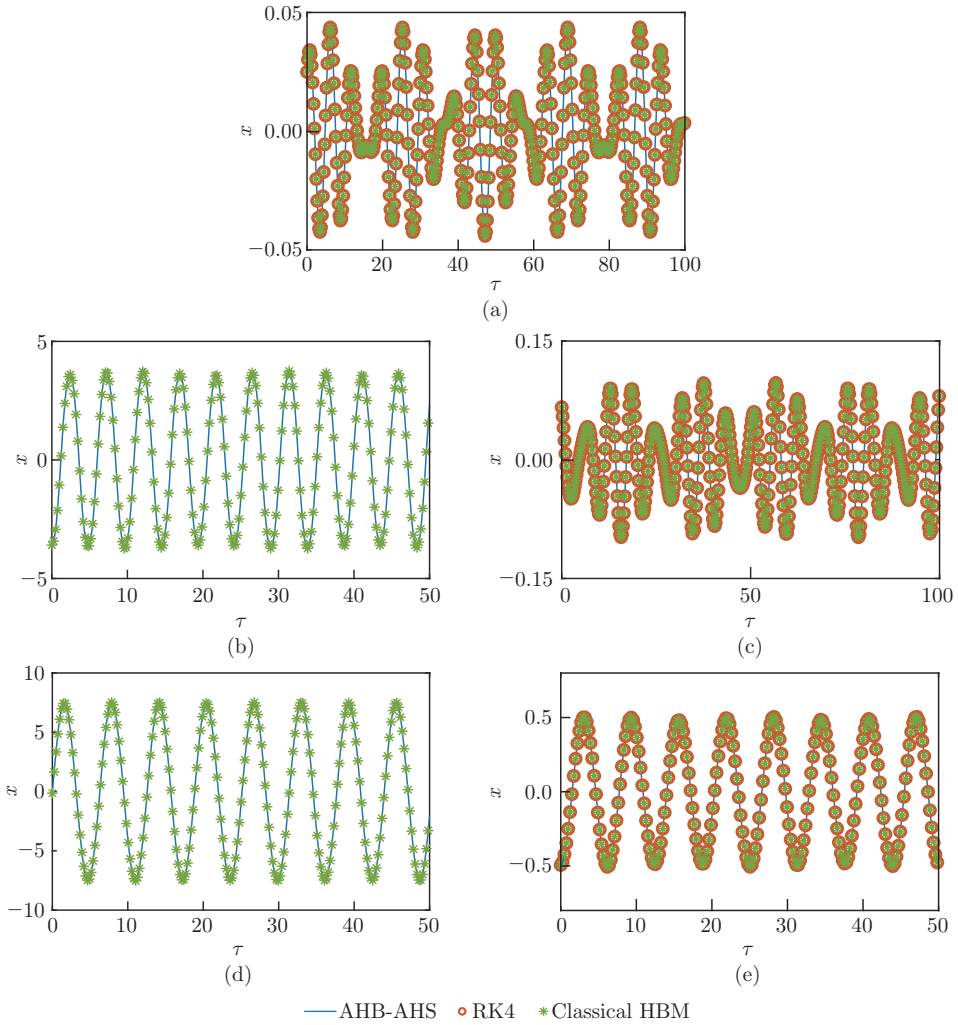

Fig. 7 Time history diagrams of different frequencies subjected to double frequency excitations: (a) $\omega = 2\,\mathrm{rad/s}$, (b) $\omega = 2.053\,\mathrm{rad/s}$ at the top of the 1st resonant peak, (c) $\omega = 3\,\mathrm{rad/s}$, (d) $\omega = 2.678\,\mathrm{rad/s}$ at the top of the 2nd resonant peak, and (e) $\omega = 3.5\,\mathrm{rad/s}$ (color online)

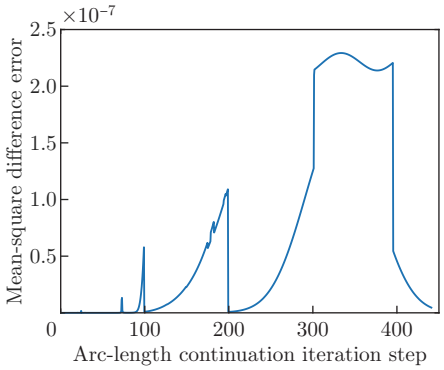

Fig. 8 Mean-square difference error of the amplitude-frequency response results obtained by the AHB-AHS method and the classical HBM subjected to double frequency excitations (color online)

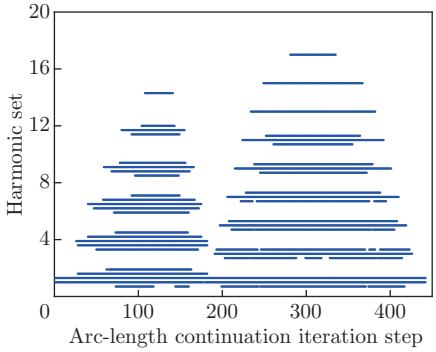

Fig. 9 Variation of the harmonic set of the generalized mathematical pendulum system subjected to double frequency excitations (color online)

resonant peak, the harmonic set is

$$\Omega = \{0.7\omega, \omega, 1.3\omega, 1.6\omega, 1.9\omega, 3.3\omega, 3.6\omega, \cdots, 7.1\omega, 8.5\omega, 9.1\omega, 9.4\omega, 11.4\omega, 11.7\omega, 12\omega, 14.3\omega\}.$$

However, at the second peak, the harmonic set becomes $\{0.7\omega, \omega, 1.3\omega, 2.7\omega, 3\omega, 3.3\omega, 4.7\omega, 5\omega, 5.3\omega, 6.7\omega, 7\omega, 7.3\omega, 8.7\omega, 9\omega, 9.3\omega, 10.7\omega, 11\omega, 11.3\omega, 13\omega, 15\omega, 17\omega\}$. Besides, the frequencies of external forces, ω and 1.3ω, are always selected, and different combination frequencies of fundamental frequencies are selected in different resonant peaks. Therefore, the AHB-AHS method is more convenient for solving the system without finding all combinations of harmonics from double frequencies.

For the calculation time, it takes 27.507 s for the AHB-AHS method to obtain the whole amplitude-frequency response curve. In comparison, the RK4 spends 79.434 s and the classical HBM spends 67.256 s on calculating the whole curve since more harmonics should be considered. The comparison of solution time by different methods is listed in Table 2.

Table 2 Calculation time of different methods for obtaining the amplitude-frequency curve of the generalized mathematical pendulum system subjected to double frequency excitations

Method	Calculation time/s	Harmonic set
AHB-AHS	27.507	Adaptive
Classical HBM	67.256	$\{0.7\omega, \omega, 1.3\omega, 2.7\omega, 3\omega, 3.3\omega, 4.7\omega, 5\omega, 5.3\omega, 6.7\omega, 7\omega, 7.3\omega, 8.7\omega, 9\omega, 9.3\omega, 10.7\omega, 11\omega, 11.3\omega, 13\omega, 15\omega, 17\omega\}$
RK4	79.434	–

3.3 Example 3: forced van der Pol system

In order to demonstrate the effect of the AHS procedure, a forced van der pol equation is considered, which is described by

$$\ddot{x} - \mu(1 - x^2)\dot{x} + x = 0.2\cos(\omega t). \tag{33}$$

If the initial harmonic set is $\{\omega\}$, the phase portrait of the van der pol equation at $\mu = 0.8$ and $\omega = 1$ is shown in Fig. 10.

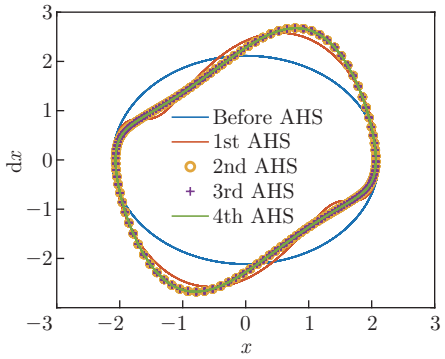

Fig. 10 Phase portraits of the van der Pol equation obtained by the AHS method when the initial harmonic set is $\{\omega\}$, where $\mu = 0.8$, and $\omega = 1$ (color online)

As is shown, the AHS procedure converged after 4 iterations. The initial harmonic set is $\{\omega\}$, which leads to the circle motion appearing in the phase portrait. The harmonic set Ω_1 after an AHS iteration is $\{\omega, 3\omega\}$, and the following harmonic set is shown in Table 3. The odd harmonics are selected to obtain the smooth limit cycle.

Table 3 Harmonics set of all AHS iterations when the initial harmonic set is $\{\omega\}$

Set	Component
Ω_0	$\{\omega\}$
Ω_1	$\{\omega, 3\omega\}$
Ω_2	$\{\omega, 3\omega, 5\omega, 7\omega, 9\omega\}$
Ω_3	$\{\omega, 3\omega, 5\omega, 7\omega, 9\omega, 11\omega, 13\omega\}$
Ω_4	$\{\omega, 3\omega, 5\omega, 7\omega, 9\omega, 11\omega, 13\omega, 15\omega\}$

If the initial harmonic set is $\{\omega, 2\omega, 3\omega, 4\omega, 5\omega\}$, which contains the unnecessary even harmonics, the results obtained by the AHB-AHS method are shown in Fig. 11. It can be seen that the number of iterations decrease to 3, and the converged limit cycle is found. The harmonic sets of all AHS iterations are shown in Table 4, where it is clear that the needless even harmonics are deleted, and new odd harmonics are added to the set Ω_1 at the first AHS iteration.

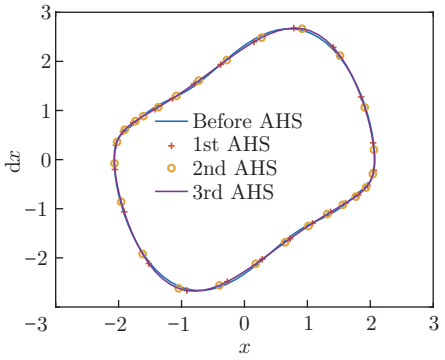

Fig. 11 Phase portraits of the van der Pol equation obtained by the AHS method when the initial harmonic set is $\{\omega, 2\omega, 3\omega, 4\omega, 5\omega\}$, where $\mu = 0.8$, and $\omega = 1$ (color online)

The comparison of the AHB-AHS method, classical HBM, and RK4 is shown in Fig. 12 and Fig. 13. As is shown, the limit cycles of different methods coincide with each other, which illustrates the accuracy of the AHB-AHS method. For the comparison of the computing efficiency

Table 4 Harmonics set of all AHS iterations when the initial harmonic set is $\{\omega, 2\omega, 3\omega, 4\omega, 5\omega\}$

Set	Component
Ω_0	$\{\omega, 2\omega, 3\omega, 4\omega, 5\omega\}$
Ω_1	$\{\omega, 3\omega, 5\omega, 7\omega, 9\omega, 11\omega\}$
Ω_2	$\{\omega, 3\omega, 5\omega, 7\omega, 9\omega, 11\omega, 13\omega\}$
Ω_3	$\{\omega, 3\omega, 5\omega, 7\omega, 9\omega, 11\omega, 13\omega, 15\omega\}$

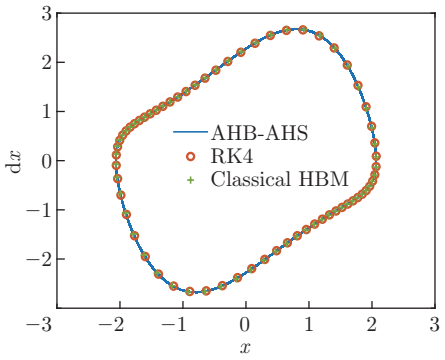

Fig. 12 Phase portraits of the van der Pol equation by different solving methods when $\mu = 0.8$, and $\omega = 1$ (color online)

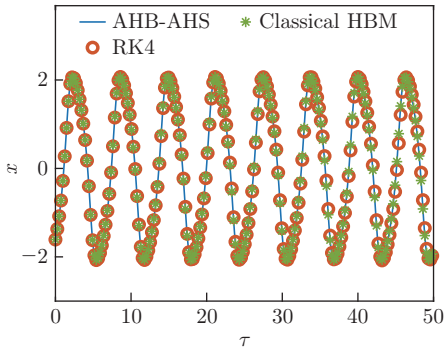

Fig. 13 Time history diagrams by different solving methods when $\mu = 0.8$, and $\omega = 1$ (color online)

of the AHB-AHS method, it takes 0.089 4 s for the AHB-AHS method to obtain the limit cycle. In comparison, the classical HBM spends 0.245 s on getting the limit cycle by choosing the 15-order harmonic truncation. The comparison of the solution time by different methods is listed in Table 5.

Table 5 Calculation time of different methods for obtaining the amplitude-frequency curve of the forced van der Pol system

Method	Calculation time/s	Harmonics set
AHB-AHS	0.089 3	Adaptive
Classical HBM	0.245 0	$\{\omega, 3\omega, \cdots, 15\omega\}$
RK4	0.563 0	–

3.4 Example 4: nonlinear Mathieu system

An advantage of the AHB-AHS method is the excellent convergence. When too many harmonics should be considered, it is difficult to find a proper initial value for carrying out the Newton iteration of classical HBM. In order to seize the initial value, generally, a linearized equation should be solved or a "brute force" method such as the direct integration method should be used to solve the nonlinear equation. To demonstrate the convergence of the AHB-AHS method, a nonlinear Mathieu equation is introduced. It is described by

$$\ddot{x} + c\dot{x} - (1 + \beta \sin t) \sin x + x^3 = 0, \tag{34}$$

which is an inverted pendulum with a rotational spring. As for the AHB-AHS method, the initial harmonic set is $\{\omega\}$, and the initial values of Fourier coefficients (a_0, a_1, b_1) are (10, 10, 10). When new harmonics are added, their initial values are all 1×10^{-2}. Therefore, they

are equivalent to the initial values (10, 10, 10, 1×10^{-2}, 1×10^{-2}, $\cdots$, 1×10^{-2}) for the classical HBM. These initial values are outrageous for the classical HBM, so the initial values will be diverged by using the classical HBM. However, it can be converged to a correct solution by means of the AHB-AHS method, and the limit cycle of the nonlinear Mathieu equation is shown in Fig. 14. It shows that the correct solution is obtained by the AHB-AHS method compared with the RK4.

The residual is defined as

$$R_{\text{es}} = \|R(x)\|_2, \tag{35}$$

where $R(x)$ is the residual vector of Eq. (8), and $\|\cdot\|_2$ is the Euclidean norm of the vector. The residual results are shown in Fig. 15. It can be seen that the residual of Eq. (8) solved by the classical HBM increases sharply. As a comparison, the residual decreases step by step until new harmonics are generated, and the initial value changes when the AHB-AHS method is applied. At the 54th, 88th, and 119th iterations (corresponding to Points A, B, and C in Fig. 15) of the Newton-Raphson method, the AHS procedure is applied, and new harmonics are generated, which makes a little disturbance to the residual. However, the iteration holds stable and continues until convergence is achieved. It is reasonable that the initial values away from the correct solution for some harmonics affect the convergence of other harmonics. The AHS procedure selects harmonics asymptotically. That is, harmonics contributing similarly to the total response are divided into a class, and are selected in an AHS iteration step. Meanwhile, the previous harmonics have been balanced, which indicates that the coefficients are close to those of the exact solution. Therefore, they lead the coefficients of new harmonics to converge to the coefficients of the exact solution.

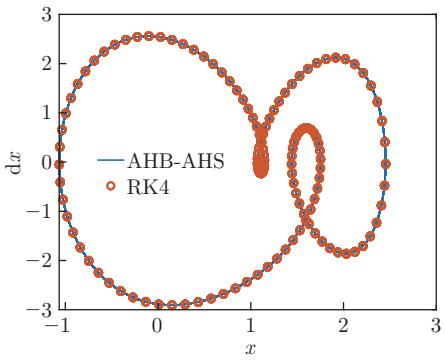

Fig. 14 Phase portraits of the nonlinear Mathieu equation when $c = 0.25$ and $\beta = 8$ with an outrageous initial value (color online)

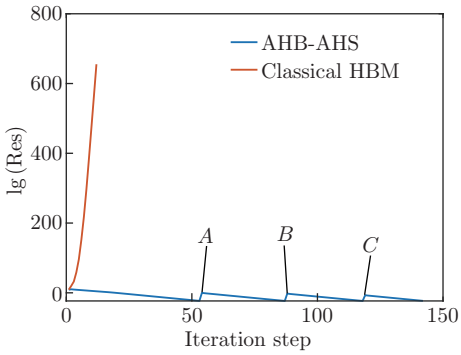

Fig. 15 Residuals of the AHB-AHS method and the classical HBM for solving the nonlinear Mathieu equation when $c = 0.25$ and $\beta = 8$ with an outrageous initial value (color online)

For the calculation time, a proper initial value is taken to make the solution of the classical HBM converge. As it is shown in Fig. 16, the solution of the AHB-AHS method agrees well with the solutions of the classical HBM and the RK4. In addition, it takes 0.138 s for the AHB-AHS method to obtain the whole amplitude-frequency response curve. In comparison, the RK4 spends 0.684 s and the classical HBM spends 0.171 s on computing the whole curve since more harmonics should be considered. The comparison of the solution time of different methods is listed in Table 6.

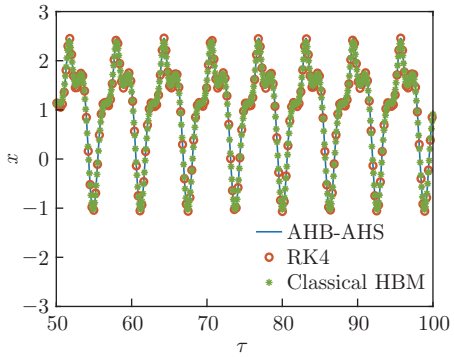

Fig. 16 Time history diagram of the nonlinear Mathieu equation when $c = 0.25$, and $\beta = 8$ (color online)

Table 6 Calculation time of different methods for obtaining the amplitude-frequency curve of the nonlinear Mathieu equation when $c = 0.25$ and $\beta = 8$

Method	Calculation time/s	Harmonic set
AHB-AHS	0.138	Adaptive
Classical HBM	0.171	$\{\omega, 2\omega, \cdots, 8\omega\}$
RK4	0.684	–

3.5 Example 5: dual rotor-bearing system

It is easy to extend the AHB-AHS method to solve multi-dimensional systems. To demonstrate the capability of the AHB-AHS method in multi-dimensional nonlinear systems, a dual rotor-bearing system is introduced. A typical dual rotor-bearing system is shown in Fig. 17. In this case, the inter-shaft bearing is modeled based on the Hertz contact theory, and the fractional exponential nonlinearity, segmentation function nonlinearity, and clearance nonlinearity are considered.

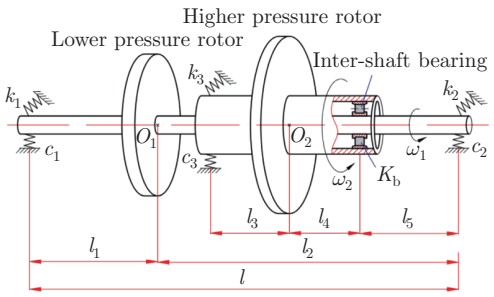

Fig. 17 Schematic diagram of the dual-rotor system with the inter-shaft bearing[42] (color online)

The dynamical equations can be expressed as

$$\begin{aligned} &m_1\ddot{x}_1 + c_1(\dot{x}_1 - \dot{\theta}_y l_1) + c_2(\dot{x}_1 + \dot{\theta}_y l_2) + k_1(x_1 - \theta_y l_1) + k_2(x_2 + \theta_y l_2) \\ &= m_1\omega_1^2 e_1 \cos(\omega_1 t) - F_{\mathrm{b}x}, \end{aligned} \tag{36a}$$

$$\begin{aligned} &m_1\ddot{y}_1 + c_1(\dot{y}_1 + \dot{\theta}_x l_1) + c_2(y_1 - \theta_x l_2) + k_1(y_1 + \theta_x l_1) + k_2(y_1 - \theta_x l_2) \\ &= m_1\omega_1^2 e_1 \sin(\omega_1 t) - F_{\mathrm{b}y} - m_1 g, \end{aligned} \tag{36b}$$

$$
\begin{aligned}
&J_{\mathrm{d}1}\ddot{\theta}_x+\omega_1 J_{\mathrm{p}1}\dot{\theta}_y+c_1l_1(\dot{y}_1+\dot{\theta}_xl_1)-c_2l_2(\dot{y}_1-\dot{\theta}_xl_2)+k_1l_1(y_1+\theta_xl_1)\\
&-k_2l_2(y_1-\theta_xl_2)\\
=&F_{\mathrm{b}y}(l_2-l_5),
\end{aligned}
\tag{36c}
$$

$$
\begin{aligned}
&J_{\mathrm{d}1}\ddot{\theta}_y-\omega_1 J_{\mathrm{p}1}\dot{\theta}_x-c_1l_1(\dot{x}_1-\dot{\theta}_yl_1)+c_2l_2(\dot{x}_1+\dot{\theta}_yl_2)-k_1l_1(x_1-\theta_yl_1)\\
&+k_2l_2(y_1+\theta_xl_2)\\
=&-F_{\mathrm{b}x}(l_2-l_5),
\end{aligned}
\tag{36d}
$$

$$
\begin{aligned}
&m_2\ddot{x}_2+c_3(\dot{x}_2-\dot{\varphi}_yl_3)+k_3(x_2-\varphi_yl_3)\\
=&m_2\omega_2^2e_2\cos(\omega_2t)+F_{\mathrm{b}x},
\end{aligned}
\tag{36e}
$$

$$
\begin{aligned}
&m_2\ddot{y}_2+c_3(\dot{y}_2+\dot{\varphi}_xl_3)+k_3(y_2+\varphi_xl_3)\\
=&m_2\omega_2^2e_2\sin(\omega_2t)+F_{\mathrm{b}y}-m_2g,
\end{aligned}
\tag{36f}
$$

$$
J_{\mathrm{d}2}\ddot{\varphi}_x+\omega_2J_{p2}\dot{\varphi}_y+c_3l_3(\dot{y}_2+\dot{\varphi}_xl_3)+k_3l_3(y_2+\varphi_xl_3)=-F_{\mathrm{b}y}l_4,
\tag{36g}
$$

$$
J_{\mathrm{d}2}\ddot{\varphi}_y-\omega_2J_{\mathrm{p}2}\dot{\varphi}_x-c_3l_3(\dot{x}_2-\dot{\varphi}_yl_3)+k_3l_3(x_2-\varphi_yl_3)=F_{\mathrm{b}x}l_4,
\tag{36h}
$$

where m, J_{d}, and J_{p} are the mass, the diameter moment of inertia, and the polar moment of inertia, respectively. The subscript 1 represents the low-pressure rotor, and the subscript 2 is the high-pressure rotor. The meanings of variables k, c, and l are shown in Fig. 17. The detailed derivation of Eq. (36) can be found in the Refs. [42] and [43]. Besides, the nonlinear forces of the inter-shaft bearing in Eq. (36) are $F_{\mathrm{b}x}$ and $F_{\mathrm{b}y}$, which can be expressed as

$$
\omega_{\mathrm{c}}=\frac{\omega_1r_{\mathrm{i}}+\omega_2r_{\mathrm{o}}}{r_{\mathrm{i}}+r_{\mathrm{o}}}=\frac{r_{\mathrm{i}}+\lambda r_{\mathrm{o}}}{r_{\mathrm{i}}+r_{\mathrm{o}}}\omega_1,
\tag{37}
$$

$$
\theta_i=\frac{2\pi}{N_{\mathrm{b}}}(i-1)+\frac{\omega_1r_{\mathrm{i}}+\omega_2r_{\mathrm{o}}}{r_{\mathrm{i}}+r_{\mathrm{o}}}t,\quad k=1,2,\cdots,N_{\mathrm{b}},
\tag{38}
$$

$$
\begin{aligned}
\delta_i=&((x_2+\theta_y(l_2-l_5))-(xl_2+\varphi_yl_4))\cos\theta_i\\
&+((y_1-\theta_x(l_2-l_5))-(y_2-\varphi_xl_4))\sin\theta_i-\delta_0,
\end{aligned}
\tag{39}
$$

$$
\begin{pmatrix}F_{\mathrm{b}x}\\F_{\mathrm{b}y}\end{pmatrix}=K_{\mathrm{b}}\sum_{i=1}^{N_{\mathrm{b}}}\delta_i^{10/9}H(\delta_i)\begin{pmatrix}\cos\theta_i\\\sin\theta_i\end{pmatrix},
\tag{40}
$$

where r_{i} and r_{o} are the radii of the inner and outer rings of the inter-shaft bearing, respectively, δ_0 is the radial clearance of the inter-shaft bearing, K_{b} is the contact stiffness, N_{b} is the number of rollers, $H(\cdot)$ represents the Heaviside function, and λ is the high and low pressure rotor speed ratio defined by

$$
\lambda=\frac{\omega_2}{\omega_1}.
$$

According to Eqs. (37)–(39), it can be seen that the nonlinear forces of the inter-shaft bearing contain piecewise function nonlinearity, fractional exponential nonlinearity, and clearance nonlinearity.

The structure parameters of the system are shown as follows:

$$\begin{cases} m_1 = 49.256\,5\,\mathrm{kg}, \quad m_2 = 55.547\,9\,\mathrm{kg}, \\ J_{\mathrm{d}1} = 0.176\,2\,\mathrm{kg}\cdot\mathrm{m}^2, \quad J_{\mathrm{p}1} = 1.521\,8\,\mathrm{kg}\cdot\mathrm{m}^2, \\ J_{\mathrm{d}2} = 0.212\,3\,\mathrm{kg}\cdot\mathrm{m}^2, \quad J_{\mathrm{p}2} = 1.038\,8\,\mathrm{kg}\cdot\mathrm{m}^2, \\ l_1 = 0.171\,95\,\mathrm{m}, \quad l_2 = 0.916\,25\,\mathrm{m}, \\ l_3 = 0.399\,30\,\mathrm{m}, \quad l_4 = 0.245\,83\,\mathrm{m}, \quad l_5 = 0.340\,47\,\mathrm{m}, \\ k_1 = k_2 = k_3 = 6\times 10^7\,\mathrm{N/m}, \\ c_1 = c_2 = c_3 = 655\,\mathrm{N}\cdot\mathrm{s/m}, \quad K_{\mathrm{b}} = 2\times 10^8\,\mathrm{N/m}^{9/10}, \\ N_{\mathrm{b}} = 19, \quad \delta_0 = 6\,\mu\mathrm{m}, \\ r_{\mathrm{i}} = 57.5\,\mathrm{mm}, \quad r_{\mathrm{o}} = 68.85\,\mathrm{mm}, \quad \lambda = 1.2. \end{cases}$$

When using the classical HBM, it is difficult to set up the harmonic set of this system. Because of the presence of the unbalanced excitation of the dual frequency and the bearing nonlinear force, the elements in the harmonic set are the permutations of the three excitation frequencies. In other words, the elements in the harmonic set can be expressed as

$$\omega_{ijk} = i\omega_1 + j\omega_2 + k\omega_{\mathrm{c}}, \quad i,j,k \in \mathbb{Z}, \tag{41}$$

where $\mathbb{Z}$ is the integer set. Assume that the maximum of each fundamental frequency is 5, i.e., $i,j,k \in [-5,5]$. Then, 11^3 frequencies are possible in the harmonic set, which will result in a significant increase in computation time and required computer memory. In general, one sets up only the harmonics of interest and ignores the other harmonics to reduce the computational effort, which undoubtedly reduces the accuracy of the solution.

In this example, the initial harmonics are set as

$$\Omega_0 = \{\omega_1, \omega_2, \omega_{\mathrm{c}}\} = \{\omega, 1.2\omega, 1.11\omega\},$$

the threshold ε is 0.001, and the sampling frequency is 128. The required frequency resolution for the three fundamental frequencies is 0.01, so the integration period should be extended to $100T$. For the classical HBM, it is difficult to calculate if all harmonics are to be considered. Therefore, we have selected 14 frequencies which, we believe, are necessary to ensure the accuracy of the classical HBM. The amplitude-frequency response curves generated by the AHB-AHS method, classical HBM, and RK4 are shown in Fig. 18. Four points A, B, C, and D are marked, respectively, and their corresponding rotational speeds are 975 rad/s, 983 rad/s, 1 176 rad/s, and 1 284 rad/s.

It can be seen that at most rotational speeds, the results obtained by the three solving methods match well. However, in two of these regions near Points B and C, the results of the AHB-AHS method and the classical HBM do not match with those of the RK4. At the resonance peak A, the RK4 cannot find the unstable solution. At the resonance peak C, all methods match well. In order to analyze the accuracy of the AHB-AHS method, the time history diagrams of the four points A, B, C, and D are drawn separately (see Fig. 19). It can be seen that the time history of Points A and C match very well, while Points B and C match better near the initial value point, and the error starts to increase with the growth of time. This phenomenon is consistent with the characteristics of chaotic motion. Therefore, the variation of the max Lyapunov exponent with the rotational speed is derived (see Fig. 20). It can be seen that the regions near Points B and C are exactly chaotic.

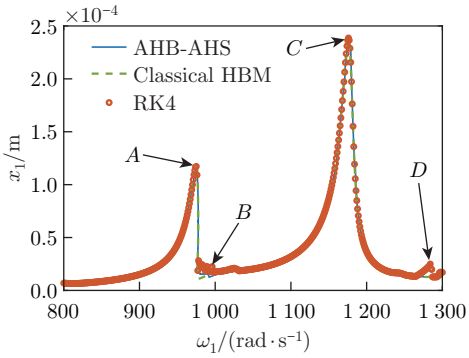

Fig. 18 Amplitude-frequency response curves of the dual rotor-bearing system (color online)

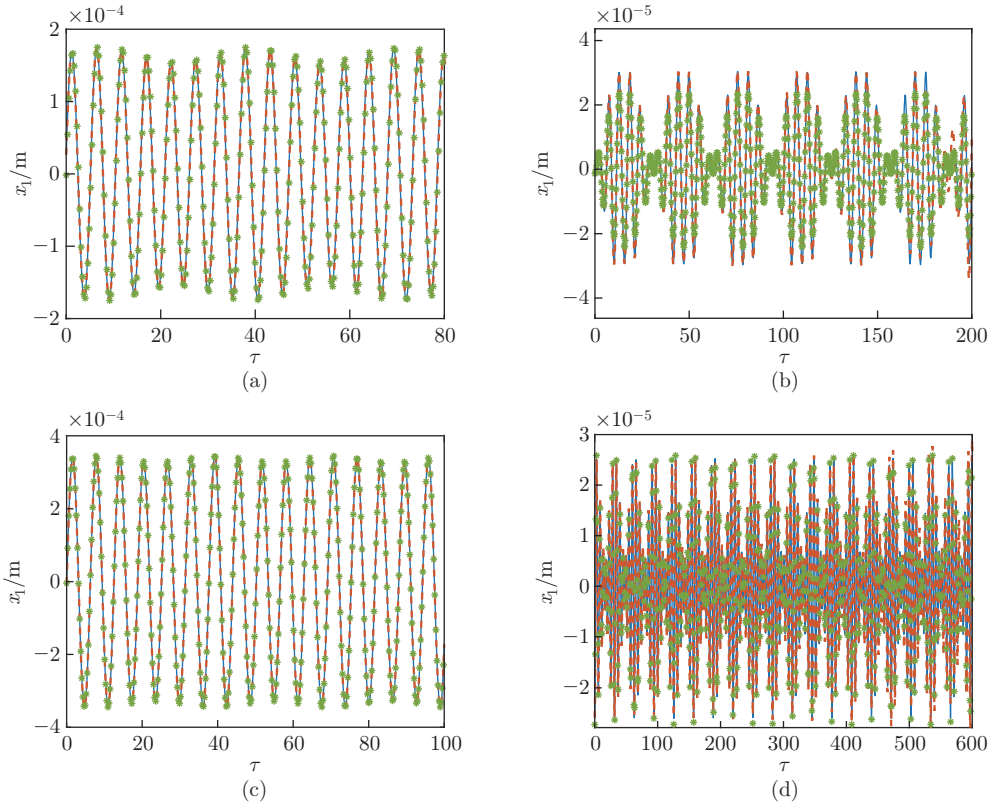

Fig. 19 Time history diagrams at different speeds (blue solid lines are for the AHB-AHS method, green asterisks are for the classical HBM, and red dashed lines are for the RK4): (a) Point A, $\omega = 975\,\mathrm{rad/s}$; (b) Point B, $\omega = 983\,\mathrm{rad/s}$; (c) Point C, $\omega = 1\,176\,\mathrm{rad/s}$; and (d) Point D, $\omega = 1\,284\,\mathrm{rad/s}$ (color online)

To demonstrate the effect of the harmonic selection by the AHB-AHS method, the variation of the harmonic set with continuation iteration is shown in Fig. 21. It can be seen that the AHS process can select different harmonics at different rotational speeds, and the harmonics increasing sharply in regions near Points B and D correspond to the continuation iteration numbers in the ranges of [350, 380] and [640, 690], respectively (see Fig. 21). In detail, 38 harmonics are selected at Point B, and 61 harmonics are selected at Point D.

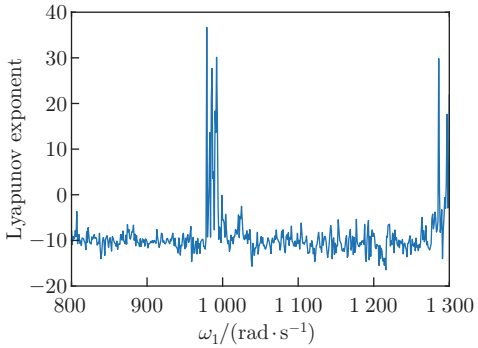

Fig. 20 Variation of the Lyapunov exponent with the rotational speed (color online)

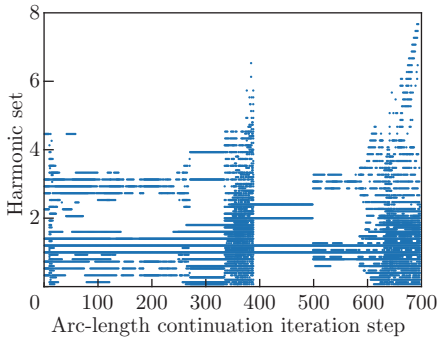

Fig. 21 Variation of the harmonic set with the arc-length continuation of the dual rotor-bearing system (color online)

The solution efficiency of the AHB-AHS method is advantageous compared with the RK4 and the classical HBM, and the calculation time of the three methods to solve the amplitude-frequency response curve is shown in Table 7. Note that we have chosen only 14 harmonics for the HBM to be calculated, because, as stated in Eq. (41), it is very difficult to solve when there are too many elements in the harmonic set. At this point, the classical HBM is slower than the AHB-AHS method, which uses more than 14 harmonics in some frequency intervals. When one does not know which harmonics to set, more harmonics will be set to ensure the accuracy of the solution, and the calculation speed of the classical HBM will be slower. In addition, due to the local convergence of the Newton iteration, it may be difficult to find a suitable initial value to converge.

Table 7 Calculation time of different methods for obtaining the amplitude-frequency curve of the dual rotor-bearing system

Method	Calculation time/s	Harmonic set
AHB-AHS	457.88	Adaptive
Classical HBM	546.14	$\{0.2\omega,\ 0.4\omega,\ 0.5\omega,\ \omega,\ 1.11\omega,\ 1.2\omega,\ 1.4\omega,\ 1.7\omega,$ $1.9\omega,\ 2\omega,\ 2.2\omega,\ 2.5\omega,\ 2.7\omega,\ 3.6\omega\}$
RK4	2 045.06	–

4 Conclusions

In this paper, a novel AHB method is developed for the nonlinear dynamic analysis. A new harmonic selection method based on the FFT is proposed to realize the adaptive selection of harmonics. Unlike most existing AHB methods, this new method does not estimate the contribution of all harmonics to the whole response, but finds the necessary harmonics from nonlinear terms and excitations. It has been shown that the new method can select harmonics asymptotically through five numerical examples. With the variation of the path parameter, some harmonics are added, and some harmonics are deleted, indicating that the harmonics are changing adaptively.

Moreover, the addition or removal of harmonics does not require a-priori knowledge of the harmonic range. Instead, the AHS procedure selects harmonics from the frequency spectra of nonlinear terms whose amplitudes are larger than a given threshold. Therefore, the AHS

procedure can select several harmonics rather than one harmonic in an iteration, which improves the efficiency of harmonic selection. Five numerical examples are used to demonstrate the calculation efficiency and accuracy of the AHB-AHS method. It is shown that the AHB-AHS method is 1.2−2.7 times faster than the classical HBM, and the mean-square difference errors between the AHB-AHS method and the classical method are smaller than 2.5×10^{-7}.

In addition, to overcome the difficulty in the number of harmonics changing in the continuation method, a modified arc-length continuation method for harmonics adaptively changing is proposed. It has been proved that all solution branches can be obtained by the modified arc-length continuation method in the first 2 numerical examples. In the 3rd example, the process of harmonic selection by the AHS procedure is shown. Besides, the convergence of the AHB-AHS method is better than that of the classical HBM in the 4th example. Although simple numerical examples are applied, the AHB-AHS method allows for handling high-dimension dynamic problems and various nonlinearities. The last numerical example shows that the AHB-AHS method can be applied to high-dimensional complex nonlinear systems. Besides, it can correctly select harmonics and solve the equations efficiently, while the traditional HBM method without harmonic selection requires solving a system of nonlinear algebraic equations of huge size, which is difficult to achieve in many cases.

Conflict of interest Yushu CHEN is an editorial board member for *Applied Mathematics and Mechanics* (*English Edition*) and was not involved in the editorial review or the decision to publish this article. The authors declare no conflict of interest.

Availability of data and materials The datasets used or analyzed during the current study are available from the corresponding author on reasonable request.

References

[1] DAI, H. H., YUE, X. K., YUAN, J. P., and ATLURI, S. N. A time domain collocation method for studying the aeroelasticity of a two dimensional airfoil with a structural nonlinearity. *Journal of Computational Physics*, **270**, 214–237 (2014)

[2] JACOB, B. P. and EBECKEN, N. F. F. An optimized implementation of the Newmarki/Newton-Raphson algorithm for the time integration of non-linear problems. *Communications in Numerical Methods in Engineering*, **10**, 983–992 (1994)

[3] EPUREANU, B. I. and DOWELL, E. H. Localized basis function method for computing limit cycle oscillations. *Nonlinear Dynamics*, **31**, 151–166 (2003)

[4] GILMORE, R. and STEER, M. Nonlinear circuit analysis using the method of harmonic balance — a review of the art, part II: advanced concepts. *International Journal of Microwave and Millimeter-Wave Computer-Aided Engineering*, **1**, 159–180 (1991)

[5] GILMORE, R. and STEER, M. Nonlinear circuit analysis using the method of harmonic balance — a review of the art, part I: introductory concepts. *International Journal of Microwave and Millimeter-Wave Computer-Aided Engineering*, **1**, 22–37 (1991)

[6] CHEN, H. Z., HOU, L., CHEN, Y. S., and YANG, R. Dynamic characteristics of flexible rotor with squeeze film damper excited by two frequencies. *Nonlinear Dynamics*, **87**, 2463–2481 (2016)

[7] GOURARY, M., ULYANOV, S., ZHAROV, M., RUSAKOV, S., GULLAPALLI, K. K., and MULVANEY, B. J. A robust and efficient oscillator analysis technique using harmonic balance. *Computer Methods in Applied Mechanics and Engineering*, **181**, 451–466 (2000)

[8] DETROUX, T., RENSON, L., MASSET, L., and KERSCHEN, G. The harmonic balance method for bifurcation analysis of large-scale nonlinear mechanical systems. *Computer Methods in Applied Mechanics and Engineering*, **296**, 18–38 (2015)

[9] SHEN, Y. J., WEN, S. F., LI, X. H., YANG, S. P., and XING, H. J. Dynamical analysis of fractional-order nonlinear oscillator by incremental harmonic balance method. *Nonlinear Dynamics*, **85**, 1457–1467 (2016)

[10] MEES, A. I. The describing function matrix. *IMA Journal of Applied Mathematics*, **10**, 49–67 (1972)

[11] SERT, O. and CIGEROGLU, E. Adaptive harmonic balance methods-a comparison. *Special Topics in Structural Dynamics*, Springer, New York, 279–289 (2016)

[12] JU, R., FAN, W., and ZHU, W. D. An efficient Galerkin averaging-incremental harmonic balance method based on the fast fourier transform and tensor contraction. *Journal of Vibration and Acoustics-Transactions of the ASME*, **142**, 061011 (2020)

[13] LAU, S. L. and CHEUNG, Y. K. Amplitude incremental variational principle for nonlinear vibration of elastic systems. *Journal of Applied Mechanics-Transactions of the ASME*, **48**, 959–964 (1981)

[14] JONES, J. C. P., YASER, K. S. A., and STEVENSON, J. Automatic computation and solution of generalized harmonic balance equations. *Mechanical Systems and Signal Processing*, **101**, 309–319 (2018)

[15] LAU, S. L., CHEUNG, Y. K., and WU, S. Y. A variable parameter incrementation method for dynamic instability of linear and nonlinear elastic systems. *Journal of Applied Mechanics-Transactions of the ASME*, **49**, 849–853 (1982)

[16] LU, W., GE, F., WU, X. D., and HONG, Y. S. Nonlinear dynamics of a submerged floating moored structure by incremental harmonic balance method with FFT. *Marine Structures*, **31**, 63–81 (2013)

[17] LEUNG, A. Y. T. and CHUI, S. K. Non-linear vibration of coupled duffing oscillators by an improved incremental harmonic balance method. *Journal of Sound and Vibration*, **181**, 619–633 (1995)

[18] HOU, L., CHEN, Y. S., FU, Y. Q., CHEN, H. Z., LU, Z. Y., and LIU, Z. S. Application of the HB-AFT method to the primary resonance analysis of a dual-rotor system. *Nonlinear Dynamics*, **88**, 2531–2551 (2017)

[19] HOU, L. and CHEN, Y. S. Analysis of 1/2 sub-harmonic resonance in a maneuvering rotor system. *Science China Technological Sciences*, **57**, 203–209 (2013)

[20] ZHANG, Z. Y., CHEN, Y. S., and LI, Z. G. Influencing factors of the dynamic hysteresis in varying compliance vibrations of a ball bearing. *SCIENCE CHINA Technological Sciences*, **58**, 775–782 (2015)

[21] SUN, C. Z., CHEN, Y. S., and HOU, L. Nonlinear dynamical behaviors of a complicated dual-rotor aero-engine with rub-impact. *Archive of Applied Mechanics*, **88**, 1305–1324 (2018)

[22] CHEN, H. Z., CHEN, Y. S., HOU, L., and LI, Z. G. Bifurcation analysis of rotor-squeeze film damper system with fluid inertia. *Mechanism and Machine Theory*, **81**, 129–139 (2014)

[23] TAGHIPOUR, J., HADDAD-KHODAPARAST, H., FRISWELL, M. I, SHAW, A. D., JALALI, H., and JAMIA, N. Harmonic-balance-based parameter estimation of nonlinear structures in the presence of multi-harmonic response and force. *Mechanical Systems and Signal Processing*, **162**, 108057 (2022)

[24] HALL, K. C., THOMAS, J. P., and CLARK, W. S. Computation of unsteady nonlinear flows in cascades using a harmonic balance technique. *AIAA Journal*, **40**, 879–886 (2002)

[25] ZHOU, S. H., SONG, G. Q., LI, Y. M., HUANG, Z. L., and REN, Z. H. Dynamic and steady analysis of a 2-DOF vehicle system by modified incremental harmonic balance method. *Nonlinear Dynamics*, **98**, 75–94 (2019)

[26] GROLL, G. and EWINS, D. J. The harmonic balance method with arc-length continuation in rotor/stator contact problems. *Journal of Sound and Vibration*, **241**, 223–233 (2001)

[27] DETROUX, T., RENSON, L., MASSET, L., and KERSCHEN, G. The harmonic balance method for bifurcation analysis of large-scale nonlinear mechanical systems. *Computer Methods in Applied Mechanics and Engineering*, **296**, 18–38 (2015)

[28] GULLAPALLI, K. K. and GOURARY, M. M. A new computational approach to simulate highly nonlinear systems by harmonic balance method. *Proceedings of the* 16*th IMACS World Congress on Scientific Computation, Applied Mathematics and Simulation*, Lausanne, Switzerland (2000)

[29] MAPLE, R. C., KING, P. I., and OXLEY, M. E. Adaptive harmonic balance solutions to Euler's equation. *AIAA Journal*, **41**, 1705–1714 (2003)

[30] MAPLE, R. C., KING, P. I., ORKWIS, P. D., and WOLFF, J. M. Adaptive harmonic balance method for nonlinear time-periodic flows. *Journal of Computational Physics*, **193**, 620–641 (2004)

[31] ZHU, L. and CHRISTOFFERSEN, C. E. Adaptive harmonic balance analysis of oscillators using multiple time scales. *The 3rd International IEEE-NEWCAS Conference*, IEEE Xplore, New York, 187–190 (2005)

[32] JAUMOUILLÉ, V., SINOU, J. J., and PETITJEAN, B. An adaptive harmonic balance method for predicting the nonlinear dynamic responses of mechanical systems-application to bolted structures. *Journal of Sound and Vibration*, **329**, 4048–4067 (2010)

[33] GROLET, A. and THOUVEREZ, F. On a new harmonic selection technique for harmonic balance method. *Mechanical Systems and Signal Processing*, **30**, 43–60 (2012)

[34] SUESS, D., JERSCHL, M., and WILLNER, K. Adaptive harmonic balance analysis of dry friction damped systems. *Nonlinear Dynamics*, **1**, 405–414 (2016)

[35] GASTALDI, C. and BERRUTI, T. M. A method to solve the efficiency-accuracy trade-off of multi-harmonic balance calculation of structures with friction contacts. *International Journal of Non-Linear Mechanics*, **92**, 25–40 (2017)

[36] SERT, O. and CIGEROGLU, E. A novel two-step pseudo-response based adaptive harmonic balance method for dynamic analysis of nonlinear structures. *Mechanical Systems and Signal Processing*, **130**, 610–631 (2019)

[37] CAMERON, T. M. and GRIFFIN, J. H. An alternating frequency/time domain method for calculating the steady-state response of nonlinear dynamic systems. *Journal of Applied Mechanics-Transactions of the ASME*, **56**, 149–154 (1989)

[38] WANG, X. F. and ZHU, W. D. A modified incremental harmonic balance method based on the fast Fourier transform and Broyden's method. *Nonlinear Dynamics*, **81**, 981–989 (2015)

[39] GUSKOV, M. and THOUVEREZ, F. Harmonic balance-based approach for quasi-periodic motions and stability analysis. *Journal of Vibration and Acoustics-Transactions of the ASME*, **134**, 031003 (2012)

[40] CHOI, S. and NOAH, S. T. Response and stability analysis of piecewise-linear oscillators under multi-forcing frequencies. *Nonlinear Dynamics*, **3**, 105–121 (1991)

[41] LINDBLAD, D., FREY, C., JUNGE, L., ASHCROFT, G., and ANDERSSON, N. Minimizing aliasing in multiple frequency harmonic balance computations. *Journal of Scientific Computing*, **91**, 65 (2022)

[42] GAO, P., HOU, L., YANG, R., and CHEN, Y. S. Local defect modelling and nonlinear dynamic analysis for the inter-shaft bearing in a dual-rotor system. *Applied Mathematical Modelling*, **68**, 29–47 (2019)

[43] CHEN, Y., HOU, L., CHEN, G., SONG, H. Y., LIN, R. Z., JIN, Y. H., and CHEN, Y. S. Nonlinear dynamics analysis of a dual-rotor-bearing-casing system based on a modified HB-AFT method. *Mechanical Systems and Signal Processing*, **185**, 109805 (2023)